

Coupling and Stacking Order of ReS₂ Atomic Layers Revealed by Ultralow-Frequency Raman Spectroscopy

Rui He,[†] Jia-An Yan,[‡] Zongyou Yin,^{||} Zhipeng Ye,[†] Gaihua Ye,[†] Jason Cheng,[†] Ju Li,^{||} and C. H. Lui^{*,‡,⊥}

[†]Department of Physics, University of Northern Iowa, Cedar Falls, Iowa 50614, United States

[‡]Department of Physics, Astronomy, and Geosciences, Towson University, Towson, Maryland 21252, United States

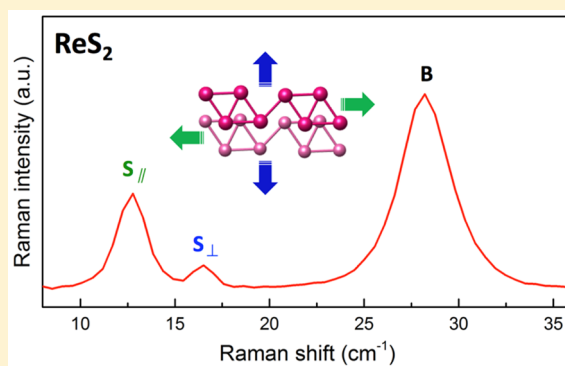
^{||}Department of Nuclear Science and Engineering and Department of Materials Science and Engineering, Massachusetts Institute of Technology, Cambridge, Massachusetts 02139, United States

[⊥]Department of Physics and Astronomy, University of California, Riverside, California 92521, United States

S Supporting Information

ABSTRACT: We investigate the ultralow-frequency Raman response of atomically thin ReS₂, a special type of two-dimensional (2D) semiconductors with unique distorted 1T structure. Bilayer and few-layer ReS₂ exhibit rich Raman spectra at frequencies below 50 cm⁻¹, where a panoply of interlayer shear and breathing modes are observed. The emergence of these interlayer phonon modes indicate that the ReS₂ layers are coupled and orderly stacked. Whereas the interlayer breathing modes behave similarly to those in other 2D layered crystals, the shear modes exhibit distinctive behavior due to the in-plane lattice distortion. In particular, the two shear modes in bilayer ReS₂ are nondegenerate and clearly resolved in the Raman spectrum, in contrast to the doubly degenerate shear modes in other 2D materials. By carrying out comprehensive first-principles calculations, we can account for the frequency and Raman intensity of the interlayer modes and determine the stacking order in bilayer ReS₂.

KEYWORDS: ReS₂, stacking order, interlayer coupling, shear mode, breathing mode, Raman



Interlayer coupling and stacking order are crucial factors to determine the physical properties in few-layer two-dimensional (2D) crystals, such as the electronic structure,¹ band gap tunability,² and quantum Hall phases.³ The interlayer coupling and stacking order are closely related to the intralayer lattice structure of the crystals. Knowledge of such correlation would allow us to tailor the material properties and possibly realize new quantum phases. However, experimental approach to this topic is challenging due to the lack of suitable materials with contrasting structure. For instance, few-layer graphene and the common transition metal dichalcogenides (TMDs), such as MoS₂ and WSe₂, possess similar stacking order due to their hexagonal in-plane lattice structure. To reveal the subtle influence of intralayer lattice on the interlayer coupling, it is imperative to explore new 2D materials with differing lattice structure.

Rhenium disulfide (ReS₂) is a new type of 2D semiconductors with intriguing properties.^{4–12} In contrast to the widely studied group-VI TMDs, such as MoS₂ and WSe₂, that possess 1H or 1T structure, ReS₂ monolayers exhibit unique distorted 1T structure as the stable phase (Figure 1a). This is because the rhenium atom possesses one extra valence electron, leading to the formation of additional Re–Re bonds in ReS₂. A superlattice structure of rhenium chains is thus formed to

distort the monolayer crystal from the more symmetric 1T phase (Figure 1a). As a consequence, the ReS₂ crystal exhibits strong in-plane anisotropy in the electronic, vibrational, and mechanical properties.^{4–9}

The in-plane distortion of ReS₂ lattice is expected to profoundly affect the interlayer coupling in few-layer ReS₂ crystals. For instance, a recent study⁴ reports that the band gap of ReS₂ remains direct from single layer (1L) to the bulk, in contrast to the direct-to-indirect band gap transition in other TMD materials. It has been suggested that the ReS₂ layers are decoupled due to the in-plane lattice distortion, which prevents ordered layer stacking and minimizes the interlayer overlap of wave functions.⁴ However, a comprehensive understanding of the layer coupling and stacking in ReS₂ is still lacking.

In this Letter, we use ultralow-frequency Raman spectroscopy to explore the interlayer coupling and stacking order of ReS₂ atomic layers. Our experiment reveals a panoply of Raman modes in the frequency range of 5–50 cm⁻¹. These Raman features arise from the interlayer shear (S) and breathing (B) phonon modes with lateral and vertical rigid layer displacement,

Received: December 2, 2015

Revised: January 2, 2016

Published: January 12, 2016



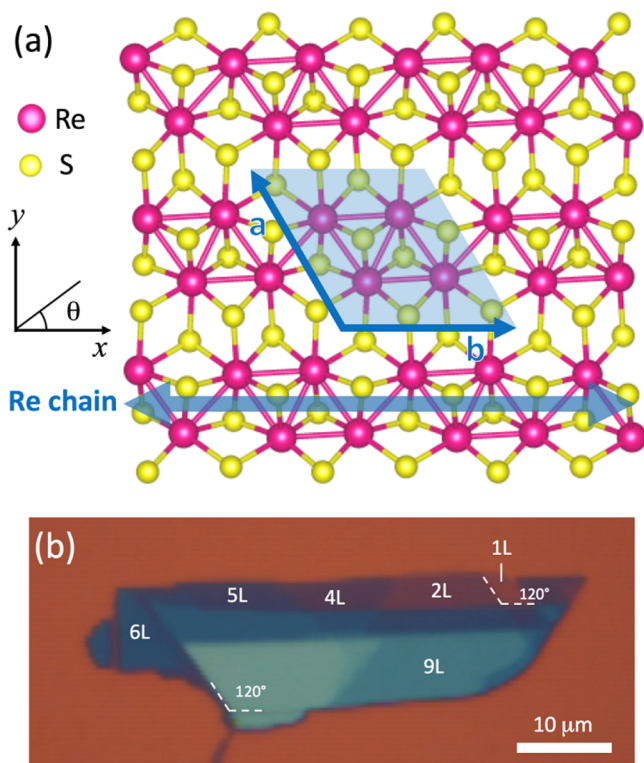


Figure 1. (a) Atomic configuration of monolayer ReS_2 with distorted 1T structure. The unit cell (blue area) contains four rhenium atoms and eight sulfur atoms. The angle between the a - and b -axis of the unit cell is 118° . We set the rhenium chain along the b -axis as the x -direction. The direction of incident light polarization is defined by the angle (θ) from the rhenium chain. (b) Optical image of an exfoliated ReS_2 sample on a Si/SiO_2 substrate. The layer numbers are denoted. Some of the cleaved edges (dashed lines) form an angle of $\sim 120^\circ$ or $\sim 60^\circ$ with one another, suggesting that they are along the a - or b -direction.

respectively. As the interlayer modes are generated directly from the coupling between individual layers, their emergence indicates non-negligible interlayer coupling and well-defined stacking order in the ReS_2 crystals. In addition, ReS_2 exhibits rich low-frequency Raman spectra with a plethora of shear modes, which are activated by the low crystal symmetry of ReS_2 . In particular, the in-plane anisotropy lifts the degeneracy between shear modes with layer displacement parallel (S_{\parallel}) and perpendicular (S_{\perp}) to the rhenium chains. The two types of shear modes are thus clearly resolved in the Raman spectra. These features contrast sharply with the two-fold degenerate shear modes observed in other 2D materials. By carrying out comprehensive first-principles calculations, we can account excellently for the frequency and Raman intensity of the interlayer modes and determine the stacking order in bilayer (2L) ReS_2 . Our findings of the layer coupling and structure of ReS_2 are critical to understand the optical and electronic properties of this material, and more generally, of all anisotropic 2D materials, including ReSe_2 , NbSe_2 and black phosphorus.

We fabricated ReS_2 samples with layer number $N = 1$ to 10 (denoted as 1L to 10L) by mechanical exfoliation of bulk ReS_2 crystals (source: 2D Semiconductors Inc.) on Si/SiO_2 substrates. The number of layers was determined by optical contrast (Figure 1b) and atomic force microscopy and further confirmed by the frequencies of the interlayer breathing modes (Figure 4). We notice that the cleaved edges of ReS_2 flakes tend

to form an angle of $\sim 120^\circ$ or $\sim 60^\circ$ with one another (dashed lines in Figure 1b), as reported by prior studies.^{5,6} These angles match well with the angle (118°) between the a - and b -axis of the unit cell in 1L ReS_2 (Figure 1a) and thus allow us to conveniently estimate the orientation of the crystal.^{5,6} The Raman spectra of these samples were measured with a commercial Horiba LabRam Raman microscope, which provides access to frequencies down to 5 cm^{-1} and spectral resolution of 0.5 cm^{-1} . A 532 nm laser with linear polarization was focused onto the samples with a spot diameter of $\sim 1 \mu\text{m}$ and incident power of $\sim 1 \text{ mW}$. The Raman signal was collected in a backscattering geometry and analyzed by the spectrometer without a polarization analyzer. We carried out the experiment in an argon-purged environment to minimize possible damage of the samples under the laser excitation.

Figure 2a displays the Raman spectra of 1L and 2L ReS_2 in a broad frequency range ($7\text{--}510 \text{ cm}^{-1}$). The 1L spectrum does not exhibit any observable Raman peaks at frequencies below 120 cm^{-1} , but a series of strong Raman features appear above 120 cm^{-1} . According to prior studies,^{4–6,11,13} these features arise from the atomic vibrations within the ReS_2 monolayer. Similar intralayer Raman modes also appear in the 2L spectrum. As the intralayer atomic bonding is much stronger than the interlayer van der Waals interactions, these high-frequency intralayer modes are insensitive to the number of layers.

At frequencies below 40 cm^{-1} , however, 2L ReS_2 exhibits three pronounced Raman peaks at 13, 16.5, and 28 cm^{-1} , which are not observed in the 1L spectrum (Figures 2a,b and 3a). Their low frequencies and absence in monolayer imply that they originate from vibrations between the two ReS_2 layers. Indeed, we expect exactly three additional interlayer vibrational modes in a 2L system, two shear modes (S) with lateral layer displacement and one layer breathing mode (B) with vertical layer displacement (Figure 3b). Because of the weak interlayer coupling, these interlayer modes generally exhibit low frequencies, as observed in other 2D materials.^{14–33} Figure 3l displays, for instance, the Raman spectrum of Bernal-stacked 2L MoS_2 , which exhibits a shear mode at 22 cm^{-1} and a breathing mode at 40 cm^{-1} . By comparing with the MoS_2 spectrum, we assign the ReS_2 Raman peak at higher frequency (28 cm^{-1}) to the breathing mode and the two peaks at lower frequencies (13 and 16.5 cm^{-1}) to the shear modes. We confirm such an assignment using more theoretical and experimental results, as will be discussed later in this paper.

Compared to other 2D materials, the interlayer modes in 2L ReS_2 exhibit a few distinctive features due to the unique distorted 1T structure. First, the two shear modes in 2L ReS_2 are nondegenerate and separate clearly for 3.5 cm^{-1} in the Raman spectrum. As we will show in our theory later, the shear modes with lower and higher frequency correspond to the normal modes with layer displacement parallel and perpendicular to the rhenium chains (S_{\parallel} and S_{\perp} modes). Although the shear modes have been generally observed in many 2D materials, their bilayers thus far exhibit no more than one shear Raman peak due to their high crystal symmetry—the two shear modes are either degenerate, such as in graphene and hexagonal TMDs,^{14–28} nearly degenerate as in NbSe_2 and ReSe_2 ,^{29,30} or Raman forbidden in the backscattering geometry for black phosphorus.^{31–33} Here for the first time, we observe nondegenerate shear modes with clear spectral separation in a bilayer 2D material.

Second, the Raman intensity of the interlayer modes varies strongly with the excitation laser polarization. We have carried

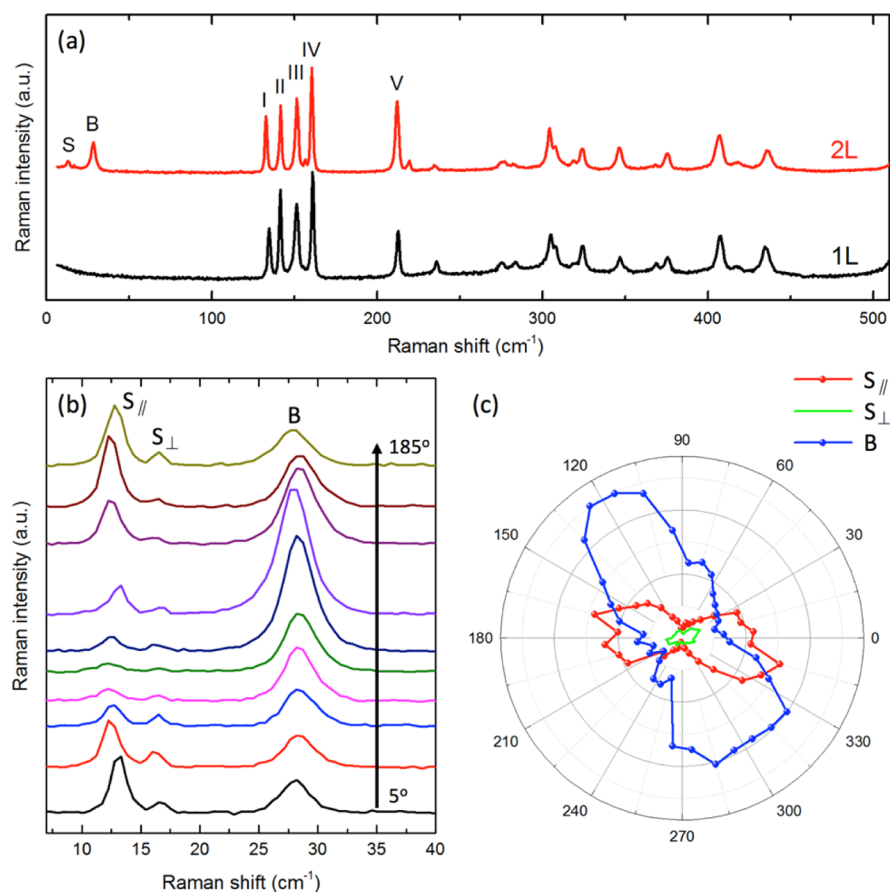


Figure 2. (a) Representative Raman spectra of ReS₂ monolayer (black) and bilayer (red). The interlayer shear modes (S) and breathing mode (B), and other intralayer modes (I–V) are denoted. (b) Raman spectra of the shear and breathing modes at different laser polarization ($\theta = 5\text{--}185^\circ$ with 20° increment). The spectra are shifted vertically for clarity. (c) The peak intensity (in arbitrary units) of the interlayer Raman modes as a function of polarization angle. In all the measurements, Raman signals of all emission polarization were collected.

out the angle-resolved Raman measurement by fixing the linear laser polarization and rotating the samples to an angle θ (inset of Figure 1a). Figure 2b,c displays the spectra and peak intensity of the interlayer modes in 2L ReS₂ as a function of θ . We select the angle, at which the Raman mode V is the strongest, as $\theta = 0$ (see Supporting Information). According to a previous Raman study by Chenet et al.,⁶ this angle corresponds to the direction of the rhenium chains in the crystal. The three interlayer modes exhibit different angular dependence. Notably, the lower-frequency shear mode is polarized approximately along the chain direction (*b*-axis) and can therefore help determine the crystal orientation.

Third, the shear modes in 2L ReS₂ are overall weaker than the layer breathing mode, as shown by the average Raman spectrum over all the polarization angles (Figure 3a). This contrasts with the results in graphene and other TMD bilayers,^{17,24–27,34} where the shear modes are stronger than the breathing mode (see, for example, the 2L MoS₂ spectrum in Figure 3l). We can understand such different behavior by considering the unit cell of the distorted 1T ReS₂ monolayer, which contains four rhenium atoms and eight sulfur atoms at somewhat irregular positions (Figure 1a). This enlarged unit cell corresponds to four identical unit cells in the 1T or 1H structure. In these more symmetric structures, the four unit cells contribute the same change of polarizability for an infinitesimal shear interlayer displacement. The total change of polarizability is thus large, resulting in a strong shear Raman

mode. For the distorted 1T ReS₂ structure, however, the corresponding four parts of the enlarged unit cell produce polarizability changes with different magnitude and signs, thus canceling one another and resulting in a smaller net change. As a result, the shear Raman modes in ReS₂ become weaker. In contrast, the layer breathing mode with out-of-plane layer displacement is hardly affected by the in-plane lattice distortion. This picture accounts qualitatively for the relatively weak shear Raman modes in ReS₂.

The observation of interlayer modes in ReS₂ provides important insight into the interlayer coupling and stacking order of this special TMD material. First, as the interlayer phonon modes are generated directly from the interlayer interaction, their emergence immediately indicates considerable lattice coupling between the ReS₂ layers. In a simple model of two coupled layers, the interlayer mode frequency (ω) is related to the monolayer mass density (μ) and the interlayer force constant (κ) as $\omega^2 = 2\kappa/\mu$. From our measured frequencies, we estimate that $\kappa = 14, 22,$ and 64×10^{18} N/m³ for the lower and higher-frequency shear modes and the breathing mode, respectively. These values are comparable to those in MoS₂ ($\kappa = 28$ and 87×10^{18} N/m³ for the shear and breathing modes, respectively, in MoS₂^{24–26}). Second, the emergence of the shear modes in ReS₂ further indicates well-defined layer stacking order in the crystal, because the generation of shear-mode vibrations requires good atomic registration between the neighboring layers. A lack of interlayer

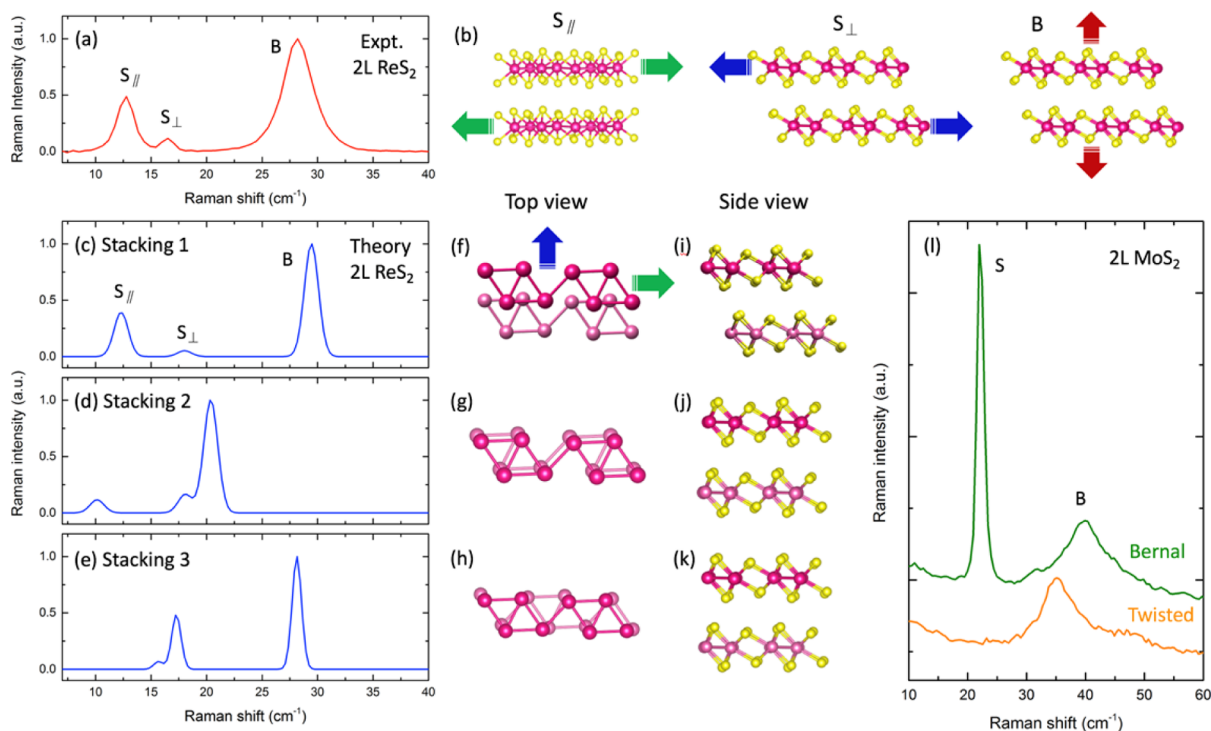


Figure 3. (a) The bilayer (2L) ReS_2 Raman spectrum averaged over all the angles in Figure 2c. (b) The schematic of the interlayer shear modes with layer displacement parallel (S_{\parallel}) and perpendicular (S_{\perp}) to the rhenium chain, as well as the interlayer breathing mode (B). (c–e) Theoretical Raman spectra of 2L ReS_2 obtained by the first-principles calculations for three stacking configurations. Stacking 1 is the most stable configuration and Stacking 2–3 are metastable. (f–k) The top view and side view of the corresponding stacking configurations to panels c–e in the same row. For clarity, only the rhenium chains are shown in the top view, and the rhenium atoms in the bottom layer are displayed with lighter color. The arrows in (f) denote the layer displacement of two shear modes, corresponding to the arrows with the same color in panel b. (l) The measured Raman spectra of 2L MoS_2 with Bernal stacking and twisted interlayer orientation for comparison with the ReS_2 spectrum in (a).

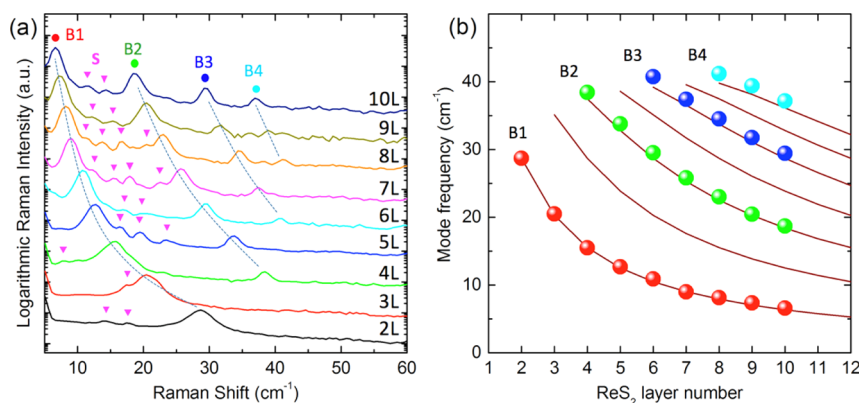


Figure 4. (a) Low-frequency Raman spectra of ReS_2 samples with layer number from 2 to 10, plotted in the logarithmic scale. We observe four sets of interlayer breathing modes (B1–B4, dots and dashed lines) and a number of weak shear modes (S, magenta triangles). (b) The breathing-mode frequency as a function of layer number. The lines are the prediction of a linear chain model, as described in the text.

lattice match will produce no overall restoring force for the lateral layer displacement. Figure 3l displays, for instance, the Raman spectrum of a twisted MoS_2 bilayer, where the breathing mode is preserved but the shear mode is eliminated. Similar lack of shear mode is also observed in other twisted TMD bilayers and heterostructures.³⁴ Our observations therefore demonstrate that the layers in ReS_2 are coupled and orderly stacked with one another.

To explore further the detailed stacking configuration of the 2L ReS_2 crystal, we have carried out comprehensive first-principles calculations with local density approximation (LDA). We first calculate the monolayer structure of ReS_2 and

determine the most stable distorted 1T structure. While fixing such monolayer structure, we calculate the total energy of the bilayer at varying interlayer displacement. We find three local energy minima in different layer displacements. At each minimum, we further relax the entire structure to reach the stable configuration (Stacking 1–3, Figure 3f–k). Among them, Stacking 1 is the most stable configuration. Stacking 2 and 3 are metastable with 30 and 7 meV higher energy per unit cell, respectively (see Supporting Information).

On the basis of these crystal configurations, we calculate the frequency and relative Raman intensity of the shear and breathing modes (Figure 3c–e). Our calculation reveals two

shear normal modes (S_{\parallel} and S_{\perp}) with interlayer displacement along and perpendicular to the rhenium chains, respectively (green and blue arrows in Figure 3b,f). The S_{\perp} mode has higher frequency than the S_{\parallel} mode, because the atomic environment varies more strongly in the perpendicular direction, resulting in larger restoring force. The Raman spectra of the three configurations are distinct from one another, indicating that the Raman response of interlayer modes is highly sensitive to the stacking order (Figure 3c–e). Remarkably, the spectrum of Stacking 1, the most stable configuration, matches excellently with our experimental spectrum, for both the mode frequencies and relative Raman intensity (Figure 3a,c).

The agreement between our theory and experiment gives us a good estimate of the stacking order of 2L ReS_2 . In our result, the top ReS_2 monolayer is displaced significantly in the direction approximately perpendicular to the rhenium chains. The whole bilayer structure looks like the Bernal stacking order in other 2D materials (Figure 3f). This stacking order is somewhat different from the triclinic structure of bulk ReS_2 crystals³⁵ but is comparable to the 2L ReS_2 layer structure observed by transmission electron microscopy.⁸ We note that as the three predicted configurations (Stacking 1–3) have quite close energy, it is possible for the stacking order to change from one into another upon external perturbation or when the layer number increases.

Thus far, our discussion is limited to 1L and 2L ReS_2 . The Raman spectra become richer and more complex for the thicker layers, as displayed in Figure 4a,b. The most prominent features of these spectra are four sets of layer breathing modes (B1–B4) (Figure 4a). Their frequencies can be well described by a linear chain model (Figure 4b)¹⁷

$$\omega_N^{(n)} = \omega_0 \cos\left(\frac{n\pi}{2N}\right) \quad (1)$$

Here N is the layer number; $n = 1, 2, \dots, N - 1$ is the mode number from high to low frequency; $\omega_0 = \sqrt{2\omega_2^{(1)}} = 39.5 \text{ cm}^{-1}$ is the extracted bulk breathing-mode frequency. Only breathing modes with $n = N - 1, N - 3, N - 5, \dots$, (every other mode from the lowest branch) are Raman active with descending Raman activity, according to symmetry analysis.¹⁷ These results are similar to those of graphene¹⁷ and other TMD layers^{24,27,28} because the breathing modes with out-of-plane layer displacement are insensitive to the in-plane lattice structure.³⁴

Besides the layer breathing modes, we also observe a panoply of Raman peaks with weaker intensity in the spectra (triangles in Figure 4a). As all of the Raman active layer breathing modes have been identified through the linear chain model, these other low-frequency Raman features must be the shear modes. An N -layer system generally possesses $2(N - 1)$ shear modes. For few-layer graphene and hexagonal TMDs, only one or two shear Raman peaks are observed because of the two-fold degeneracy and Raman selection rules of the shear modes.^{14,17,24,27,28} In few-layer ReS_2 with lower crystal symmetry, however, all the shear modes are Raman active with no degeneracy. Their spectra contain rich information about the crystalline structure of few-layer ReS_2 . However, it is not an easy task to explore all of these shear modes, because they are generally weak and easily blocked by the stronger breathing modes. Only those shear modes with relatively strong signal and nonoverlapping frequencies are observed in our experiment. Their frequencies also appear to be somewhat irregular due to the in-plane lattice distortion. Further research

is merited to understand the complex interlayer Raman modes in ReS_2 .

In conclusion, we have investigated the interlayer phonon modes in bilayer and few-layer ReS_2 by ultralow-frequency and angle-resolved Raman spectroscopy. Our results and analysis reveal intriguing interlayer coupling and stacking order in this special type of 2D materials with distorted 1T structure. The knowledge of their layer structure and coupling should facilitate our understanding of their optical and electronic properties. The results and methods in our study are also crucial to understand the properties of other 2D materials with in-plane anisotropy, such as ReSe_2 , NbSe_2 , and black phosphorus.

Upon the completion of this work, we became aware of three similar Raman studies by other groups.^{36–38} Some observed different Raman spectra for the interlayer modes in ReS_2 , which may reflect the different stacking order in the ReS_2 crystals, as predicted by our theoretical calculation.

■ ASSOCIATED CONTENT

Supporting Information

The Supporting Information is available free of charge on the ACS Publications website at DOI: 10.1021/acs.nanolett.5b04925.

The polarization-dependent Raman spectra of the low and high-frequency phonon modes in bilayer ReS_2 , as well as the detailed description of our first-principles calculations. (PDF)

■ AUTHOR INFORMATION

Corresponding Author

*E-mail: joshua.lui@ucr.edu.

Notes

The authors declare no competing financial interest.

■ ACKNOWLEDGMENTS

We thank H. Sahin for discussion and B. S. M. Leong and J. Valdecanas for assistance in data analysis. R.H. acknowledges support from ACS Petroleum Research Fund (Grant 53401-UNI10) and NSF (Grant DMR-1410496). J.A.Y. acknowledges the Faculty Development and Research Committee Grant (OSPR No. 140269) and the FCSM Fisher General Endowment at Towson University. Z.Y. and J.L. acknowledge support by NSF DMR-1410636.

■ REFERENCES

- (1) Mak, K. F.; Shan, J.; Heinz, T. F. *Phys. Rev. Lett.* **2010**, *104*, 176404.
- (2) Lui, C. H.; Li, Z.; Mak, K. F.; Cappelluti, E.; Heinz, T. F. *Nat. Phys.* **2011**, *7*, 944–947.
- (3) Zhang, L.; Zhang, Y.; Camacho, J.; Khodas, M.; Zaliznyak, I. *Nat. Phys.* **2011**, *7*, 953–957.
- (4) Tongay, S.; Sahin, H.; Ko, C.; Luce, A.; Fan, W.; Liu, K.; Zhou, J.; Huang, Y.-S.; Ho, C.-H.; Yan, J.; Ogletree, D. F.; Aloni, S.; Ji, J.; Li, S.; Li, J.; Peeters, F. M.; Wu, J. *Nat. Commun.* **2014**, *5*, 3252.
- (5) Liu, E.; Fu, Y.; Wang, Y.; Feng, Y.; Liu, H.; Wan, X.; Zhou, W.; Wang, B.; Shao, L.; Ho, C.-H.; Huang, Y.-S.; Cao, Z.; Wang, L.; Li, A.; Zeng, J.; Song, F.; Wang, X.; Shi, Y.; Yuan, H.; Hwang, H. Y.; Cui, Y.; Miao, F.; Xing, D. *Nat. Commun.* **2015**, DOI: 10.1002/adfm.201504546.
- (6) Chenet, D. A.; Aslan, O. B.; Huang, P. Y.; Fan, C.; van der Zande, A. M.; Heinz, T. F.; Hone, J. C. *Nano Lett.* **2015**, *15*, 5667–5672.
- (7) Corbet, C. M.; McClellan, C.; Rai, A.; Sonde, S. S.; Tutuc, E.; Banerjee, S. K. *ACS Nano* **2015**, *9*, 363–370.

- (8) Lin, Y.-C.; Komsa, H.-P.; Yeh, C.-H.; Björkman, T.; Liang, Z.-Y.; Ho, C.-H.; Huang, Y.-S.; Chiu, P.-W.; Krasheninnikov, A. V.; Suenaga, K. *ACS Nano* **2015**, *9*, 11249–11257.
- (9) Zhong, H.-X.; Gao, S.; Shi, J.-J.; Yang, L. *Phys. Rev. B: Condens. Matter Mater. Phys.* **2015**, *92*, 115438.
- (10) Zhang, E.; Jin, Y.; Yuan, X.; Wang, W.; Zhang, C.; Tang, L.; Liu, S.; Zhou, P.; Hu, W.; Xiu, F. *Adv. Funct. Mater.* **2015**, *25*, 4076–4082.
- (11) Feng, Y.; Zhou, W.; Wang, Y.; Zhou, J.; Liu, E.; Fu, Y.; Ni, Z.; Wu, X.; Yuan, H.; Miao, F.; Wang, B.; Wan, X.; Xing, D. *Phys. Rev. B: Condens. Matter Mater. Phys.* **2015**, *92*, 054110.
- (12) Yu, Z. G.; Cai, Y.; Zhang, Y.-W. *Sci. Rep.* **2015**, *5*, 13783.
- (13) Wolverson, D.; Crampin, S.; Kazemi, A. S.; Ilie, A.; Bending, S. J. *ACS Nano* **2014**, *8*, 11154–11164.
- (14) Tan, P. H.; Han, W. P.; Zhao, W. J.; Wu, Z. H.; Chang, K.; Wang, H.; Wang, Y. F.; Bonini, N.; Marzari, N.; Pugno, N.; Savini, G.; Lombardo, A.; Ferrari, A. C. *Nat. Mater.* **2012**, *11*, 294–300.
- (15) Lui, C. H.; Malard, L. M.; Kim, S.; Lantz, G.; Laverge, F. E.; Saito, R.; Heinz, T. F. *Nano Lett.* **2012**, *12*, 5539–5544.
- (16) Lui, C. H.; Heinz, T. F. *Phys. Rev. B: Condens. Matter Mater. Phys.* **2013**, *87*, 121404(R).
- (17) Lui, C. H.; Ye, Z.; Keiser, C.; Xiao, X.; He, R. *Nano Lett.* **2014**, *14*, 4615–4621.
- (18) Lui, C. H.; Ye, Z.; Keiser, C.; Barros, E. B.; He, R. *Appl. Phys. Lett.* **2015**, *106*, 041904.
- (19) Boschetto, D.; Malard, L.; Lui, C. H.; Mak, K. F.; Li, Z.; Yan, H.; Heinz, T. F. *Nano Lett.* **2013**, *13*, 4620–4623.
- (20) Cong, C. C.; Yu, T. Y. *Nat. Commun.* **2014**, *5*, 4709.
- (21) Tan, P.-H.; Wu, J.-B.; Han, W.-P.; Zhao, W.-J.; Zhang, X.; Wang, H.; Wang, Y.-F. *Phys. Rev. B: Condens. Matter Mater. Phys.* **2014**, *89*, 235404.
- (22) Zeng, H.; Zhu, B.; Liu, K.; Fan, J.; Cui, X.; Zhang, Q. M. *Phys. Rev. B: Condens. Matter Mater. Phys.* **2012**, *86*, 241301(R).
- (23) Plechinger, G.; Heydrich, S.; Eroms, J.; Weiss, D.; Schüller, C.; Korn, T. *Appl. Phys. Lett.* **2012**, *101*, 101906.
- (24) Zhao, Y.; Luo, X.; Li, H.; Zhang, J.; Araujo, P. T.; Gan, C. K.; Wu, J.; Zhang, H.; Quek, S. Y.; Dresselhaus, M. S.; Xiong, Q. *Nano Lett.* **2013**, *13*, 1007–1015.
- (25) Zhang, X.; Han, W. P.; Wu, J. B.; Milana, S.; Lu, Y.; Li, Q. Q.; Ferrari, A. C.; Tan, P. H. *Phys. Rev. B: Condens. Matter Mater. Phys.* **2013**, *87*, 115413.
- (26) Boukhicha, M.; Calandra, M.; Measson, M.-A.; Lancry, O.; Shukla, A. *Phys. Rev. B: Condens. Matter Mater. Phys.* **2013**, *87*, 195316.
- (27) Chen, S.-Y.; Zheng, C.; Fuhrer, M. S.; Yan, J. *Nano Lett.* **2015**, *15*, 2526–2532.
- (28) Froehlicher, G.; Lorchat, E.; Fernique, F.; Joshi, C.; Molina-Sánchez, A.; Wirtz, L.; Berciaud, S. *Nano Lett.* **2015**, *15*, 6481–6489.
- (29) Xi, X.; Zhao, L.; Wang, Z.; Berger, H.; Forró, L.; Shan, J.; Mak, K. F. *Nat. Nanotechnol.* **2015**, *10*, 765–769.
- (30) Zhao, H.; Wu, J.; Zhong, H.; Guo, Q.; Wang, X.; Xia, F.; Yang, L.; Tan, P.; Wang, H. *Nano Res.* **2015**, *8*, 3651–3661.
- (31) Ling, X.; Liang, L.; Huang, S.; Puzos, A. A.; Geohegan, D. B.; Sumpter, B. G.; Kong, J.; Meunier, V.; Dresselhaus, M. S. *Nano Lett.* **2015**, *15*, 4080–4088.
- (32) Luo, X.; Lu, X.; Koon, G. K. W.; Castro Neto, A. H.; Özyilmaz, B.; Xiong, Q.; Quek, S. Y. *Nano Lett.* **2015**, *15*, 3931–3938.
- (33) Dong, S.; Zhang, A.; Liu, K.; Ji, J.; Ye, Y. G.; Luo, X. G.; Chen, X. H.; Ma, X.; Jie, Y.; Chen, C.; Wang, X.; Zhang, Q. *arXiv:1503.06577* **2015**.
- (34) Lui, C. H.; Ye, Z.; Ji, C.; Chiu, K.-C.; Chou, C.-T.; Andersen, T. I.; Means-Shively, C.; Anderson, H.; Wu, J.-M.; Kidd, T.; Lee, Y.-H.; He, R. *Phys. Rev. B: Condens. Matter Mater. Phys.* **2015**, *91*, 165403.
- (35) Lamfers, H. J.; Meetsma, A.; Wieggers, G. A.; de Boer, J. L. *J. Alloys Compd.* **1996**, *241*, 34–39.
- (36) Nagler, P.; Plechinger, G.; Schüller, C.; Korn, T. *Phys. Status Solidi RRL* **2015**, 9999, n/a.
- (37) Lorchat, E.; Froehlicher, G.; Berciaud, S. *arXiv:1512.03842* **2015** (accessed Jan. 13, 2015).
- (38) Qiao, X.-F.; Wu, J.-B.; Zhou, L.-W.; Qiao, J.-S.; Shi, W.; Chen, T.; Zhang, X.; Zhang, J.; Ji, W.; Tan, P. H. *arXiv:1512.08935* **2015** (accessed Jan. 13, 2015).

Supporting Information for “Coupling and stacking order of ReS₂ atomic layers revealed by ultralow-frequency Raman spectroscopy”

Rui He[†], Jia-An Yan[‡], Zongyou Yin[¶], Zhipeng Ye[†], Gaihua Ye[†], Jason Cheng[†],
Ju Li[¶], and C. H. Lui^{⊥*}

[†]Department of Physics, University of Northern Iowa, Cedar Falls, Iowa 50614, USA

[‡]Department of Physics, Astronomy and Geosciences, Towson University, Towson, Maryland 21252, USA

[¶]Department of Nuclear Science and Engineering and Department of Materials Science and Engineering, Massachusetts Institute of Technology, Cambridge, Massachusetts 02139, USA

[⊥]Department of Physics and Astronomy, University of California, Riverside, California 92521, USA

*Corresponding author: joshua.lui@ucr.edu

I. Angle-resolved Raman measurement for bilayer ReS₂

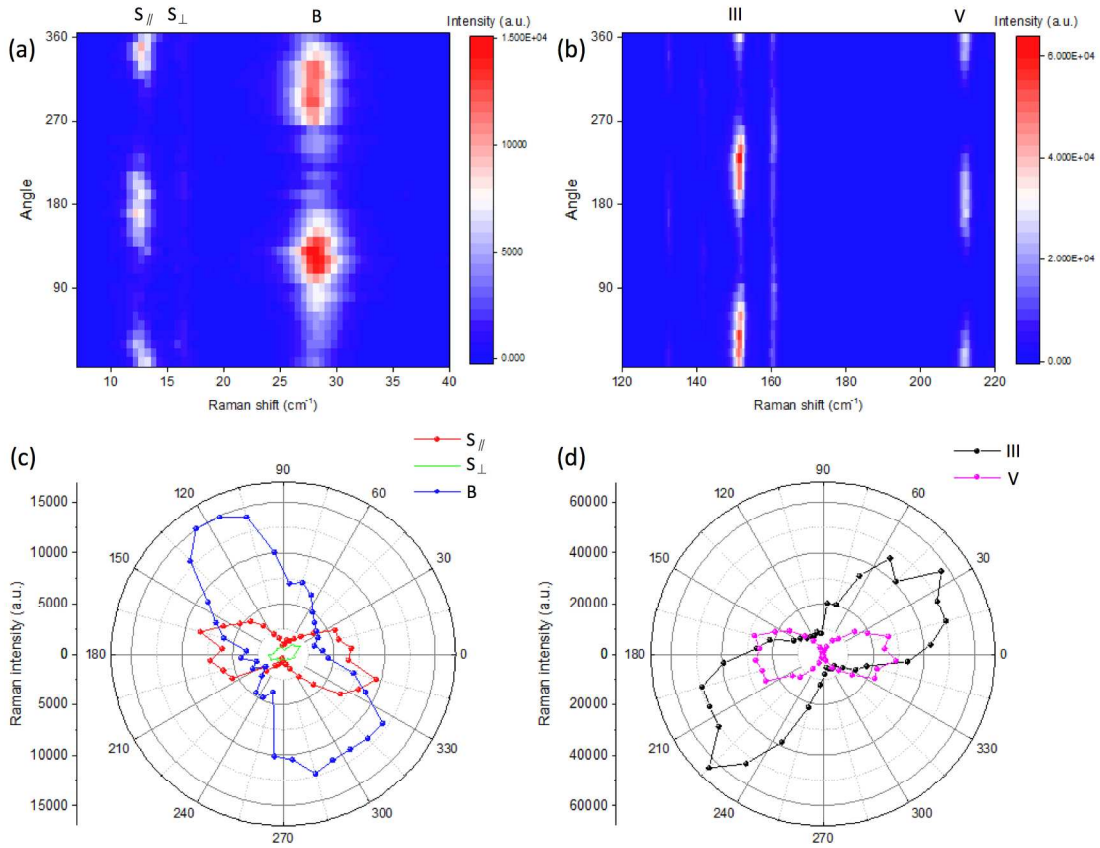


Figure S1. (a-b) Color maps of the Raman spectra of the interlayer shear and breathing modes (a) and the intralayer modes (b) at varying rotation angle in 2L ReS₂. (c-d) The peak intensity of the shear and breathing modes (c), Mode III and V (d) as a function of rotation angle. We define the angle at which Mode V reaches the maximum intensity as the zero angle. Panel (c) is the same as Figure 2(c) in the main paper.

We have carried out the angle-resolved Raman measurement on bilayer (2L) ReS₂. In the measurement, we fixed the linear incident laser polarization and rotated the sample. The Raman signals of all emission polarization were collected at varying rotation angle θ . The angle θ is defined in the inset of Figure 1(a) of the main paper. Figure S1 (a-b) display the 2D color maps

of the interlayer shear and breathing modes and the intralayer modes (III, V). Figure S1 (c-d) display the peak intensity of these modes as a function of θ . We select the angle, at which the Mode V is the strongest, as $\theta = 0$. According to a previous Raman study by Chenet *et al* [1], this angle corresponds to the direction of the rhenium chains in the crystal.

II. First-principles calculations for monolayer ReS₂

First-principles calculations based on density-functional theory (DFT) [2,3] were performed using the Quantum ESPRESSO (QE) code [4] with the Perdew-Zunger (PZ) local density approximation (LDA) exchange-correlation functional. For comparison, we also carried out calculations using the generalized gradient approximation (GGA) with Perdew-Burke-Ernzerhof (PBE) parametrization [5,6]. Norm-conserving pseudopotentials were employed for the description of interactions between the core and valence electrons. The cutoff energy in the plane wave expansion was set to 50 Ry. A shifted Monkhorst-Pack uniform k -grid of $8 \times 8 \times 1$ was adopted for all self-consistent calculations. A vacuum region of more than 20 Å was introduced along the out-of-plane direction to eliminate spurious interactions among the periodic images. All the atomic structures and unit cells have been fully relaxed until the stress along each axis is smaller than 0.5 kbar and the forces on the atoms are smaller than 0.003 eV/Å. After the crystal structure was fully relaxed, we further calculated the electronic band structure and phonon frequencies at the Brillouin zone center. The non-resonant Raman intensity of each phonon mode was then obtained using the density-functional perturbation theory as implemented in QE. Similar method has been applied to study the strain effect on the Raman response of monolayer (1L) MoS₂ [7]

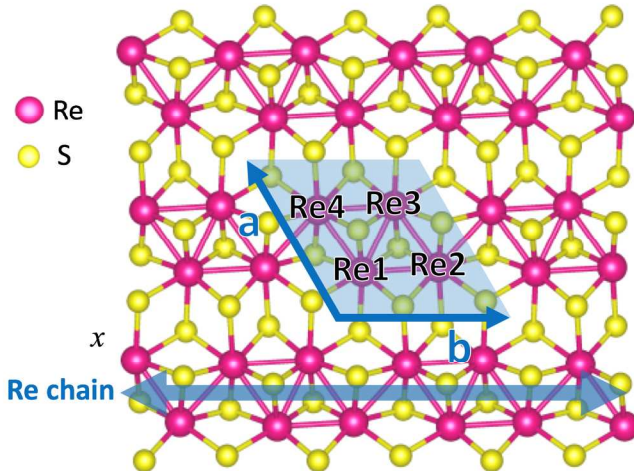


Figure S2. The crystallographic structure of 1L ReS₂. The four rhenium atoms, labeled as Re1, Re2, Re3 and Re4, form a diamond structure, which lines up as a chain along the b -direction.

Figure S2 displays the fully relaxed crystallographic structure of 1L ReS₂. There are 12 atoms in the unit cell, including four rhenium atoms labeled as Re1, Re2, Re3 and Re4. These rhenium atoms form a diamond structure that lines up as a linear chain, giving rise to strong in-plane anisotropy in the crystal. The bond lengths between these rhenium atoms are listed in Table S1. We note that 1L ReS₂ possesses inversion symmetry, from which all the other unlisted bond lengths can be readily obtained. Our calculated bond lengths agree well with the previous

theoretical and experimental results [8-11]. We note that our calculations predict a relatively short distance between the Re1 and Re3 atoms, indicating strong bonding between them.

Parameters in 1L ReS ₂	LDA	GGA
a	6.489 Å	6.643 Å
b	6.320 Å	6.477 Å
γ	119.86°	119.85°
Re1-Re2	2.782 Å	2.845 Å
Re1-Re4	2.776 Å	2.855 Å
Re1-Re3	2.690 Å	2.755 Å
Re2-Re4	4.864 Å	4.990 Å

Table S1. Calculated LDA and GGA lattice parameters (**a**, **b**), their angle (γ), and bond lengths between different rhenium atoms in 1L ReS₂. The rhenium atoms (Re1 - Re4) are denoted in Figure S2.

Mode No.	LDA	GGA	Expt.
1	128.0	130.5	135.2
2	138.1	135.1	141.8
3	156.3	149.6	150.4
4	164.5	158.6	160.9
5	222.8	206.6	211.6
6	242.6	229.4	227.8
7	268.2	261.7	234.7
8	277.9	268.1	275.8
9	302.3	292.1	282.9
10	306.3	295.4	305.8
11	311.2	301.8	319.2
12	320.8	307.2	324.2
13	345.6	331.4	346.8
14	365.3	340.8	368.7
15	373.8	354.9	375.1
16	405.1	392.1	407.1
17	413.9	403.2	417.4
18	431.8	419.3	435.5

Table S2. Calculated LDA and GGA frequencies (in cm⁻¹) of the 18 Raman-active A_g modes in 1L ReS₂. Experimental data are listed for comparison.

ReS₂ has a symmetry point group of C_i . The irreducible representations of the 36 Γ -point vibrational modes can be decomposed as $18(A_g+A_u)$, including 18 non-degenerate Raman-active A_g modes, 3 acoustic A_u modes and 15 infrared-active A_u modes. Table S2 lists the frequencies of all the 18 Raman-active modes calculated by LDA and GGA. The calculated frequencies agree well with our experimental data, as well as with previous theoretical results.

We have also calculated the electronic band structure of 1L ReS₂ with LDA and GGA (Figures S3). Our LDA calculations predict a direct energy gap of 1.569 eV at the Γ point but a slightly smaller indirect gap of 1.532 eV near the Γ point, with 37 meV energy difference [Figure S3(a)]. The GGA calculations yield similar results, in which the indirect gap (1.424 eV) is slightly below the direct gap (1.431 eV) with 7 meV energy difference [Figure S3(b)]. These results are somewhat different from those of prior studies that predicted a direct gap in 1L ReS₂ [8]. We note, however, that the energy difference between the direct and indirect gap is rather small in our calculation, and may not produce observable effect in experiments at room temperature. Experiments at low temperature are needed to reveal the fine features of the band structure in 1L ReS₂.

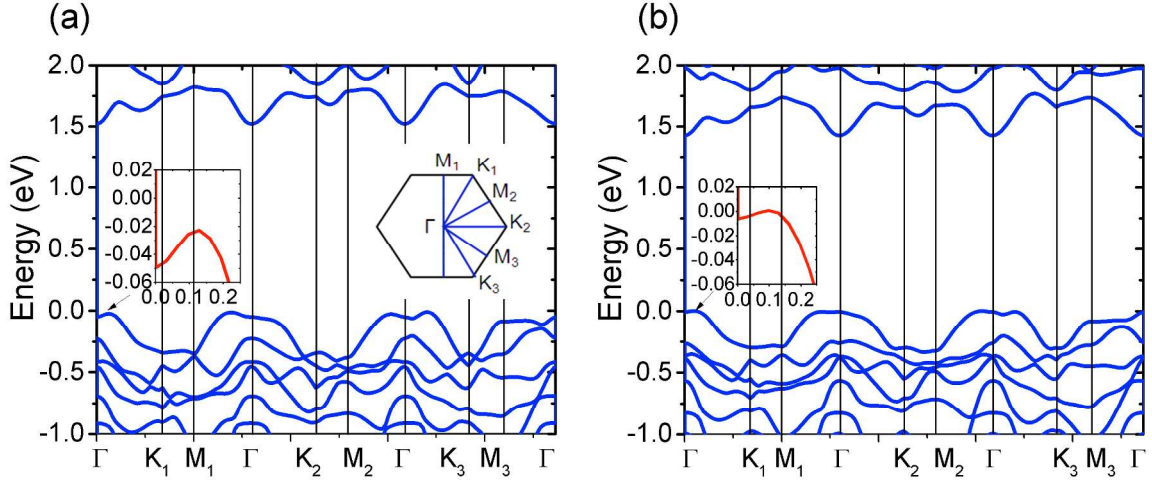


Figure S3. Electronic band structure of 1L ReS₂ calculated from (a) LDA and (b) GGA. The insets show the zoom-in view near the Γ point and the symmetry points in the first Brillouin zone.

III. First-principles calculations for bilayer ReS₂

Based on our results of 1L ReS₂, we carried out comprehensive calculations for the stacking geometry and the Raman response of 2L ReS₂. Since LDA yields reasonable results for the crystal structure, electronic band structure and Raman spectra of other atomically thin transition metal dichalcogenides (TMDs) [12], here we present our LDA results for 2L ReS₂. Recent transport and TEM experiments have demonstrated strong in-plane anisotropy in few-layer ReS₂. These results indicate that the rhenium chains in different ReS₂ layers are aligned parallel to one another. In view of this observation, here we only consider the translational layer displacement in 2L ReS₂, and neglect any possible rotation of the layers.

We started with two ReS₂ monolayers, which are on top of each other with identical crystal orientation. We then shifted them laterally in a direction perpendicular to the rhenium chain, and calculated the energy of the bilayer system as a function of the rigid layer displacement (d)

[Figure S4 (a-c)]. In this first stage of calculation, we kept the monolayer crystal structure unchanged and only minimized the interlayer energy. We found three local minima in our results [Position 1-3 in Figure S4 (c)]. Afterward, for each of these local minima, we fully relaxed the entire structure (including the monolayer lattice) to reach the most stable configuration [Stacking 1-3 in Figure S4(d-f)]. Our final results (Table S3) show that Stacking 1 is the most stable configuration, and Stacking 2 and 3 are metastable. The energies of Stacking 2 and 3 are, respectively, 30 and 7 meV per unit cell higher than that of Stacking 1. The energy differences are quite small if we consider that there are totally 24 atoms in the unit cell of 2L ReS₂. The ReS₂ layers are therefore expected to exhibit different stacking order at different external conditions. We note that Stacking 2 is close to the triclinic layer structure of bulk ReS₂ crystals [13]. This stacking order is, however, not the most stable one for the bilayer.

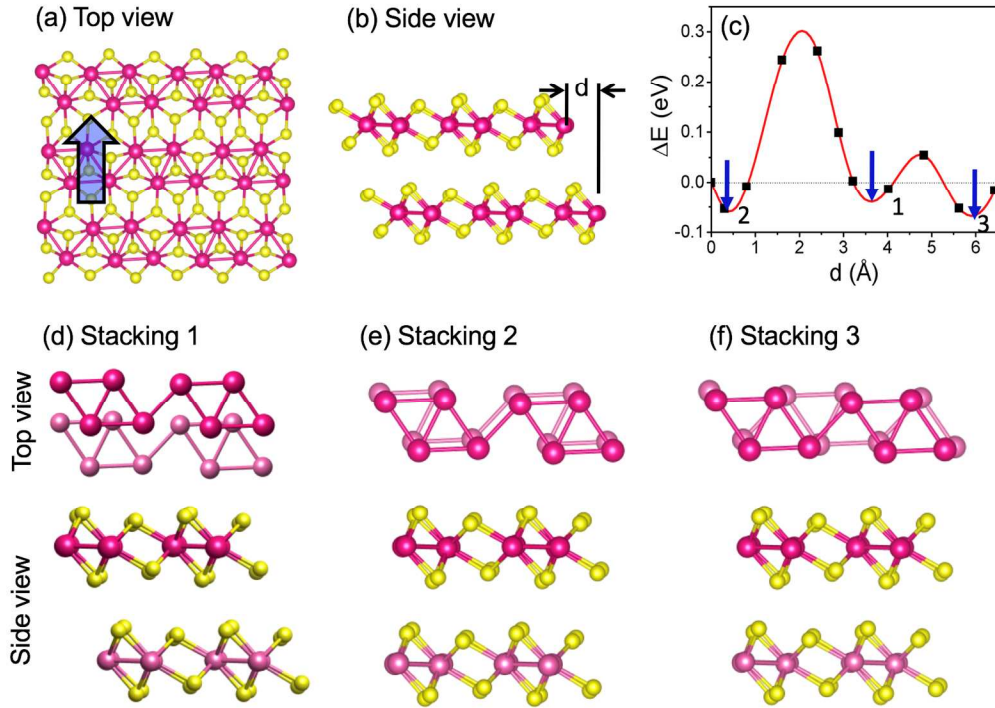


Figure S4. (a) Top view and (b) side view of the rigid shift of the top layer with respect to the bottom layer along the direction perpendicular to the Re-chain in 2L ReS₂. (c) Energy variation as a function of the layer displacement (d) in 2L ReS₂. Three energy minima are identified from the energy curve. (d-f) The corresponding top view and side view of the fully relaxed atomic structures at positions 1-3 in Panel (c). The final relative displacement vectors are listed in Table S3.

Stacking	Energy (meV)	a (Å)	b (Å)	γ	\vec{d} (Å)
1	0	6.501	6.329	119.89°	(0.00, 2.17, 6.04)
2	30.0	6.501	6.329	119.87°	(-0.28, -0.39, 6.03)
3	7.7	6.506	6.335	119.90°	(-0.01, -5.92, 5.94)

Table S3. Calculated total energy per unit cell, lattice parameters, and relative displacements \vec{d} between the top and bottom layers for three different stacking configurations of 2L ReS₂.

We have further calculated the Raman spectra of all three stacking configurations. Figure 5(a)-(c) show their Raman spectra in the high frequency range. Although the phonon modes of different stacking configurations exhibit different Raman intensities, their frequencies are very similar. This result is expected, because the high-frequency phonon modes are mainly generated by intralayer atomic interactions and are thus insensitive to the layer stacking geometry. The calculated Raman spectra in the low frequency range ($<40 \text{ cm}^{-1}$) are shown in Figure 3 of the main paper. The three different stacking configurations yield distinct low-frequency Raman response, because the interlayer phonon modes are sensitive to the stacking order. Only the Raman spectrum of Stacking 1 matches our experimental spectrum. This is consistent with our energetic analysis, which shows that Stacking 1 is the most stable configuration. We have also calculated the electronic band structure for all three stacking configurations in 2L ReS₂ [Figure S5(d)-(f)]. All of them exhibit direct band gap at the Γ point.

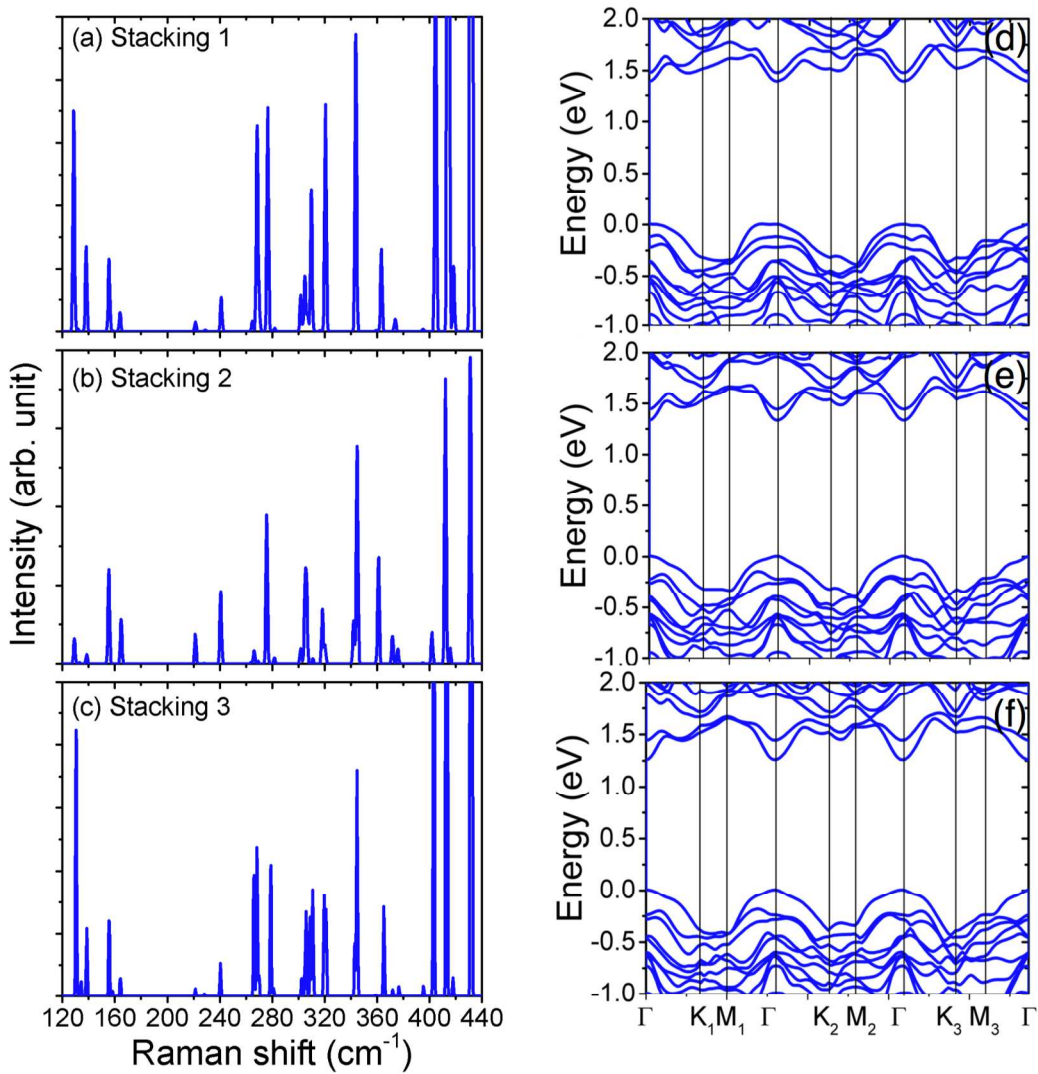


Figure S5. Simulated high-frequency ($120 - 440 \text{ cm}^{-1}$) Raman spectra for (a) Stacking 1, (b) Stacking 2 and (c) Stacking 3, and (d-f) their corresponding electronic band structure. The Fermi level is set to the top of the valence band in (d-f).

Finally, we comment on the validity of our calculated Raman spectra using QE. Our results correspond to the spatial average over all the polarizations. To double check the validity of this approach, we have also calculated the Raman spectra for two basic polarization configurations, the $z(xy)-z$ and $z(xx)-z$ configurations, based on the obtained Raman tensors. In all cases, the x -direction is selected to be along the b -axis of the crystal. As shown in Figure S6, the results agree well with the direct output from QE.

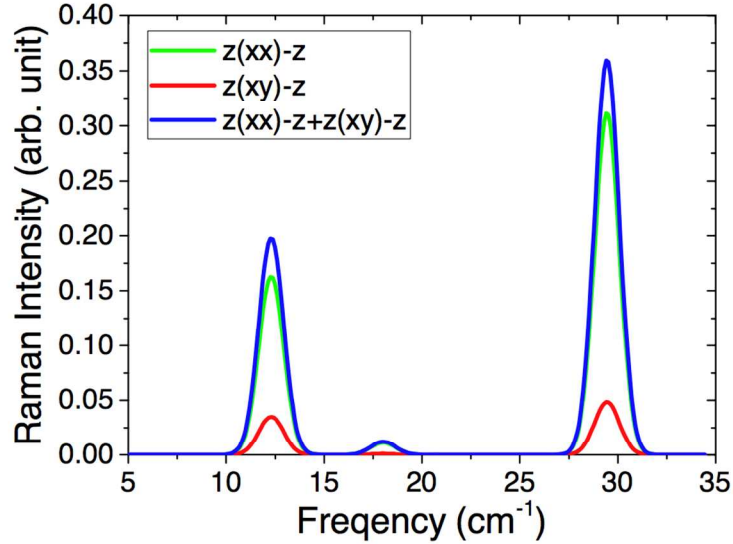


Figure S6. Calculated Raman spectra of bilayer ReS_2 in different polarization geometry. The x -direction is selected to be along the b -axis of the ReS_2 crystal.

Supporting references:

- [1] D. A. Chenet *et al.*, Nano Lett. **15**, 5667 (2015).
- [2] P. Hohenberg and W. Kohn, Phys. Rev. **136**, B864 (1964).
- [3] W. Kohn and L. J. Sham, Phys. Rev. **140**, A1133 (1965).
- [4] G. Paolo *et al.*, Journal of Physics: Condensed Matter **21**, 395502 (2009).
- [5] J. P. Perdew, K. Burke, and M. Ernzerhof, Phys. Rev. Lett. **77**, 3865 (1996).
- [6] J. P. Perdew, K. Burke, and M. Ernzerhof, Phys. Rev. Lett. **78**, 1396 (1997).
- [7] D. Doratotaj, J. R. Simpson, and J.-A. Yan, arXiv:1511.04280 (2015).
- [8] S. Tongay *et al.*, Nat. Commun. **5**, 3252 (2014).
- [9] H.-X. Zhong, S. Gao, J.-J. Shi, and L. Yang, Phys. Rev. B **92**, 115438 (2015).
- [10] Y.-C. Lin *et al.*, ACS Nano **9**, 11249 (2015).
- [11] Y. Feng *et al.*, Phys. Rev. B **92**, 054110 (2015).
- [12] H. Terrones *et al.*, Scientific Reports **4**, 4215 (2014).
- [13] H. J. Lamfers, A. Meetsma, G. A. Wiegers, and J. L. de Boer, Journal of Alloys and Compounds **241**, 34 (1996).